NMR Structure of the N-SH2 of the p85 Subunit of Phosphoinositide 3-Kinase Complexed to a Doubly Phosphorylated Peptide Reveals a Second Phosphotyrosine Binding Site†

Tanja Weber,‡ Brian Schaffhausen,§ Yuxi Liu,§ and Ulrich L. Günther*,‡

Institut für Biophysikalische Chemie, J. W. Goethe Universität, Frankfurt, Biozentrum N230, Marie-Curie-Strasse 9, 60439 Frankfurt, Germany, and Department of Biochemistry, Tufts University School of Medicine, 136 Harrison Avenue, Boston, Massachusetts 02111

Received June 27, 2000; Revised Manuscript Received September 25, 2000

ABSTRACT: The N-terminal src homology 2 (SH2) domain of the p85 subunit of phosphoinositide 3-kinase (PI3K) has a higher affinity for a peptide with two phosphotyrosines than for the same peptide with only one. This unexpected result was not observed for the C-terminal SH2 from the same protein. NMR structural analysis has been used to understand the behavior of the N-SH2. The structure of the free SH2 domain has been compared to that of the SH2 complexed with a doubly phosphorylated peptide derived from polyomavirus middle T antigen (MT). The structure of the free SH2 domain shows some differences from previous NMR and X-ray structures. In the N-SH2 complexed with a doubly phosphorylated peptide, a second site for phosphotyrosine interaction has been identified. Further, line shapes of NMR signals showed that the SH2 protein−ligand complex is subject to temperature-dependent conformational mobility. Conformational mobility is also supported by the spectra of the ligand peptide. A binding model which accounts for these results is developed.

Phosphatidylinositol 3-kinases (PI3Ks)[1] are broadly important in cell function (*1*−*9*). PI3Ks are important for mitogenic signaling (*10*, *11*), vesicle trafficking (*4*, *6*), cell movement (*12*), rearrangement of cytoskeletal actin (*13*), and chemotaxis (*14*). Activation is also associated with acute stimulation such as platelet activation by thrombin (*15*, *16*), stimulation of neutrophils by fMet-Leu-Phe (*17*), and stimulation of phagocytosis (*18*). PI3K has an important role in preventing apoptosis in a variety of cell types (*19*). Finally, PI3K activation is associated with tumor invasion (*20*). Major forms of PI3K are heterodimers consisting of a catalytic 110 kDa subunit and an 85 kDa regulatory subunit (*21*). The regulatory p85 subunit contains two SH2 domains. These domains are responsible for interactions of PI3K with tyrosine phosphorylated sequences of oncogenes such as middle T (*22*) or receptors such as the platelet-derived growth factor receptor (PDGFr) (*23*, *24*).

The src homology 2 (SH2) domains of p85 are representatives of modules found in over 100 proteins (*25*−*28*). SH2 domains are sequences of approximately 100 amino acids that bind phosphorylated (usually tyrosine) sequences. Since many proteins are tyrosine phosphorylated, specificity is a critical issue. Residues C-terminal to the phosphotyrosine (pTyr) of the ligand are particularly important in this regard (*29*). A large number of SH2 structures determined by both X-ray and NMR methods (see, for example, the review in ref *30*) have provided structural explanations for specificity.

This work extends our NMR analysis on the N-terminal SH2 domain of the regulatory subunit of phosphatidylinositol 3-kinase. The focus here is on interactions of the SH2 domain with doubly tyrosine phosphorylated ligands. Closely spaced tyrosine phosphorylation sites have been observed in a number of different SH2 signaling contexts. Immunoreceptor tyrosine-based activation motifs (ITAM) loosely defined by the consensus sequence YXXLX6−8YXXL, where X is any amino acid, have been identified in signaling subunits of the T and B cell antigen receptors, the high-affinity Fc receptor for IgE (FcR), and other FcRs (*31*, *32*).

Clustering of ITAM-containing receptors results in phosphorylation of the two critical tyrosine residues in the ITAM which converts it into a high-affinity ligand that interacts with tandem SH2 domains of members of the Syk/ZAP-70 family of tyrosine kinases (*31*, *32*). Closely spaced phosphorylation sites are also found in non-ITAM-containing receptors such as the insulin or PDGF receptors. The spacing is more variable than for ITAM motifs. In the case of the

† This work was supported by a grant from the Deutsche Forschungsgemeinschaft (DFG) and by grants from the NIH (B.S.) as well as by BASF Bioresearch.

* To whom correspondence should be addressed: telephone, 49-(0)69-79829623; fax, 49-(0)69-79829632; e-mail, ugunt@bpc.uni-frankfurt.de.

‡ J. W. Goethe Universität, Frankfurt.

§ Tufts University School of Medicine.

[1] Abbreviations: N-SH2, N-terminal src homology 2 domain of p85; C-SH2, C-terminal SH2 domain; PI3K, phosphoinositide 3-kinase; MT, polyomavirus middle T antigen; PDGFr, platelet-derived growth factor receptor; pTyr, phosphotyrosine; ITAM, Immunoreceptor tyrosine-based activation motif; PLCγ1, phospholipase C γl; ESI, electrospray ionization; MALDI, matrix-assisted laser desorption ionization; GST, gluthatione *S*-transferase; NOESY, nuclear Overhauser effect spectroscopy; TOCSY, total correlation spectroscopy; MT8/315pY, EEEpYMPME-NH_2; MT15/315pY, EEEpYMPMEDLYLDIL-NH_2; MT15/315pY/322pY, EEEpYMPMEDLpYLDIL-NH_2; HSQC, heteronuclear single-quantum coherence; Grb2, growth factor receptor bound protein 2.

10.1021/bi001474d CCC: $19.00
Published on Web 11/30/2000

PDGF receptors, these two sites are 740 and 751. In the insulin receptor there are six residues between two YXXM motifs, while in IRS 1 there are 20. In the viral oncogene polyoma middle T, residues 315 and 322 are tyrosine phosphorylated (*33*−*35*).

Such closely spaced sites could potentially serve different kinds of functions. In polyoma middle T, tyrosine 315 is the major site for interaction with PI3K (*36*, *37*), while tyrosine 322 can support association with PLCγl (*38*). More interesting possibilities arise from association of doubly tyrosine phosphorylated sequences with multiple SH2s in the same protein. The structures of ITAM motifs−SH2 interactions show ways in which this can be achieved (*39*−*41*). Activation of PI3K *in vitro* works much better with doubly phosphorylated peptides than with monophosphorylated ones (*42*−*45*). One thought is that using two tyrosine phosphorylations and two SH2s is a method for enhancing the affinity of interactions. However, evidence has also been presented that diphosphotyrosine sequences can induce oligomerization of PI3K (*46*).

This work examines the solution structure of the N-terminal SH2 domain of PI3K bound to a doubly phosphorylated peptide from polyoma middle T antigen. It shows a novel mechanism for SH2 interactions in which a second phosphotyrosine participates in ligand binding. Line shapes of NMR signals are presented which demonstrate temperature-dependent conformational mobility induced by the doubly phosphorylated ligand. These data are used to discuss an extended model for SH2−ligand interaction.

MATERIALS AND METHODS

All peptides including the doubly phosphorylated peptide EEEpYMPMEDLpYLDIL-NH_2 were synthesized and HPLC purified by the Tufts Protein Chemistry Facility as described earlier (*47*). The purity of the doubly phosphorylated peptide was confirmed by NMR spectra and ESI and MALDI mass spectra, which showed doubly phosphorylated peptide with no single or unphosphorylated peptide present. Binding assays have also been described previously (*47*, *48*). Briefly, tyrosine phosphorylated middle T was prepared by immunoprecipitation from Sf9 cells infected with MT and c-src expressing baculoviruses and in vitro labeling with [γ-^{32}P]-ATP (2000 Ci/mmol, NEN). For competition experiments, p85 N-SH2 fusion protein on glutathione beads was incubated with competitor for 30 min at 4 °C. ^{32}P-labeled middle T was added and the mixture incubated for 1 h on ice. Washed samples were analyzed by SDS−PAGE. The gels were stained with Coomassie Brilliant Blue to measure fusion protein and analyzed using a Molecular Dynamics phosphorimager to determine bound labeled middle T.

Protein samples were expressed as described previously (*47*, *48*) using 1 L of CELTONE-CN (MARTEK Biosciences Corp.). The concentration of the SH2 samples was approximately 1.5 mM. In the case of the complex a reduced sample volume of 220 μL was used in a SHIGEMI NMR tube. NMR spectra were recorded at 500 and 600 MHz. Sequential assignments for the free SH2 were initially obtained from ^{15}N-edited NOESY (*49*) and TOCSY (*50*) spectra and later confirmed and completed by HNCA (*51*) and HN(CO)CA (*52*). Side chain assignments were primarily obtained from CC(CO)NH and HCC(CO)NH (*53*) but also from HCCH-TOCSY (*54*) experiments. Distance constraints were obtained from ^{15}N- and ^{13}C-edited NOESY (*49*) spectra recorded at 500 and 600 MHz.

NOESY assignments were obtained by a semiautomatic procedure employing a program from Pristovsek (*55*). Lists of all peaks derived from ^{15}N- and ^{13}C-edited NOESY spectra were compared automatically to the chemical shift values of all atoms and preliminarily assigned. The output was filtered against existing structures. The obtained distance constraints were directly incorporated into DYANA distance geometry calculations, and rejected distance constraints were eliminated before a second DYANA run. Resulting structures were again used for subsequent filtering steps where again all NOESY constraints were allowed. Tolerances in this filtering process were chosen large enough to accept new assignments varying from the given structure. This process converged after 10−15 iterations when the RMSD between structures of different filtering stages and those of one DYANA run became equal. The final assignments were probed by manual inspection of NOESY signals.

Initial calculations for the protein complex included only intramolecular constraints. The observed intermolecular NOEs derived from ^{13}C{F_1}-filtered 2D NOESY spectra (*56*, *57*) were incorporated into the structure calculation after the protein fold had already converged in the absence of the ligand. Structures were energy minimized with MSI DISCOVER employing the final constraints obtained by the filtering process and manual inspection.

RESULTS

The SH2−ligand model used here is the p85 N-SH2 of PI3K associating with peptide sequences from polyomavirus middle T (MT). The ability of MT to activate PI3K is broadly important for the ability of the virus to cause a wide variety of tumors (*58*). The association of MT and PI3K depends on tyrosine phosphorylation at residue 315 (*59*). Tyrosine phosphorylated middle T associated with either N-terminal or C-terminal SH2 domains cloned from rat PI3K (*22*). The N-terminal SH2 domain construct used in these studies has 114 residues. It has a serine residue at βD4 compared to a leucine found in p85 SH2s used in other structural studies (*60*, *61*). This SH2 has been used in a wide range of binding and structural studies (*22*, *47*, *48*, *62*). For example, chemical shift analysis has been used to monitor interactions between the SH2 and a number of tyrosine phosphorylated peptides (*47*). One standard binding assay measures the ability of phosphorylated peptides to block the binding of ^{32}P-labeled tyrosine phosphorylated middle T to GST-p85 N-SH2 fusion protein immobilized on glutathione beads (*22*, *47*, *48*). This assay was used to show the large contributions of the pTyr 315 as well as the first and third residues C-terminal to this pTyr in the MT sequence (EEEpY_{315}MPME) to the ability of peptides to compete with MT for binding to the N-SH2 (*47*).

Middle T is known to have a second tyrosine phosphorylation site at residue 322 (*33*, *59*). The effect of phosphorylation at this site was determined using longer peptides [EEEpYMPMEDL(p)YLDIL-NH_2]. Table 1A compares the ability of the singly phosphorylated middle T sequence (EEEpYMPMEDLYLDIL-NH_2, MT15/315pY) and the doubly phosphorylated sequence (EEEpYMPMEDLpYLDIL-

Table 1: Comparison of the Ability of the Middle T Phosphopeptides MT15/315pY/322Y and MT15/315pY/322pY To Compete with Middle T Binding to p85 N-SH2 (A) and p85 C-SH2 (B)[a]

	(A) p85 N-SH2 peptide competitor concn (μM)				
	0.0	12.5	4.2	1.4	0.5
none	1.0[b]				
315pY/322Y		0.22	0.45	0.76	nd[c]
315pY/322pY		nd	0.13	0.23	0.56
	(B) p85 C-SH2 peptide competitor concn (μM)				
	0.0	12.5	2	0.4	0.08
none	1.0[b]				
315pY/322Y		0.07	0.16	0.51	0.82
315pY/322pY		0.07	0.16	0.51	0.89

[a] GST-N-SH2 was incubated with peptide for 30 min at 4 °C prior to addition of ^{32}P tyrosine phosphorylated middle T. After middle T addition, incubation was continued for an additional 60 min. After being washed, bound middle T was determined by SDS−PAGE and Phosphorimager analysis. [b] Relative ^{32}P counts. No peptide addition was given the value of 1.0. The other ^{32}P counts are given relative to this control value. [c] Not detectable.

NH_2, MT15/315pY/322pY) to compete with middle T for binding to the p85 N-SH2. It required approximately 9 times as much singly phosphorylated peptide to achieve the same competition as the doubly phosphorylated peptide. To ask whether this is a general effect of having a second phosphate, the same kind of experiment was carried out using a C-terminal SH2 construct (Table 1B). For the p85 C-SH2 construct, there was no difference in the ability of the two peptides to compete. These results suggest that the N-SH2 domain has some site that is capable of interacting with the second tyrosine phosphate. This observation provided the impetus for the structural studies described here.

Our previous work (*47*) used HSQC analysis for evaluating SH2−peptide interactions. A more complete structural analysis was needed to examine the complex with the doubly tyrosine phosphorylated peptide. Figure 1 shows 20 superimposed structures of the free N-SH2 obtained by distance geometry and subsequent energy minimization and a corresponding Richardson diagram. The structure is well-defined for residues corresponding to positions 330−430 of the p85 sequence (RMSD of 1.71 ± 0.24 Å for all atoms and 0.92 ± 0.15 Å for the backbone). Residues of the BC loop (361−365) were not observed in this wild-type SH2 or in a series of p85 N-SH2 mutants, and there were consequently no structural constraints for this region. A similar situation has also been observed by Booker for the bovine p85 N-SH2 (*63*). A better RMSD (all atoms, 1.54 ± 0.23 Å; backbone, 0.78 ± 0.15 Å) is obtained when the unassigned residues 361−365 are not included in the RMSD calculation.

The p85 N-SH2 consists of the usual central β-sheet, an additional small sheet, and two flanking α-helices (Figure 1). There are some differences between this structure and those determined previously by either NMR (*63*) or X-ray (*61*). For example, X-ray diffraction shows an N-terminal α-helix that is not seen in any of the NMR structures. The most striking difference between the two NMR structures is found in the BG loop region. The overall fold of the BG loop is similar in both NMR structures, but here A414 and K423 adopt conformations that move the whole loop toward the bulk of the protein. In the structure determined by Booker the BG loop was more isolated from the bulk of the protein. Our structure in this region is closer to that determined by Nolte using X-ray diffraction. The cause of all these differences may be that older NMR structures were mainly based on constraints derived from ^{15}N-edited spectra where the number of NOE distance constraints is limited and constraints are only observed between backbone NH protons and side chain protons in spatially proximal side chains. Clearly, there was some uncertainty about the BG loop in the earlier structure, because assignments of residues between 418 and 420 were missing even in a later structural paper from the same group (*60*). The work here employs ^{13}C-NOESY-HSQC spectra that result in a much larger set of distance restraints, including constraints between side chain signals. In fact, most constraints (58) between the BG loop and the bulk of the protein stem from the ^{13}C-NOESY spectrum while only 16 constraints were observed between backbone and side chain resonances.

Additional, more subtle differences between the two NMR structures include a slightly stronger twist in the large central triple β-sheet of our NMR structure. The C-terminal part of βD turns away more quickly from the central β-sheet toward the EF loop. Thus there is now an angle of 30° between βD′

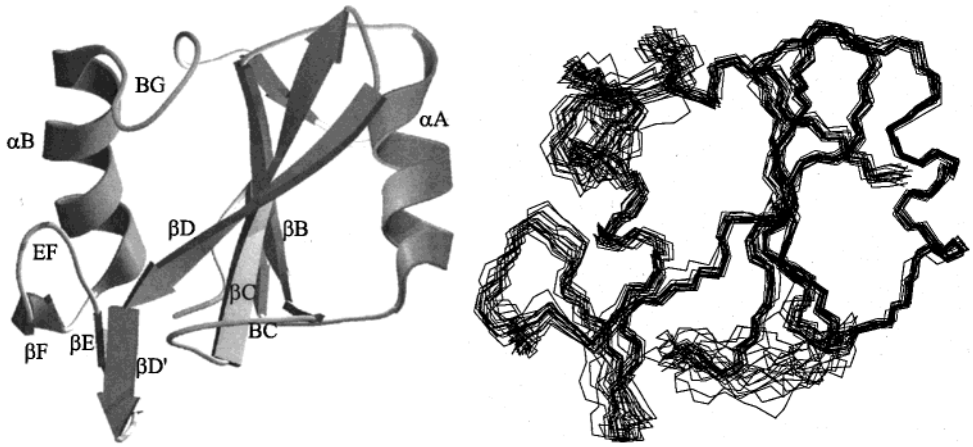

FIGURE 1: Left: Richardson diagram of the uncomplexed PI3K p85 N-SH2 NMR structure. The naming of structural elements follows the description of Eck et al. (*71*). Right: Superposition of the C^{α}, C′, and N backbone atoms of 20 structures obtained after distance geometry and energy minimization. These figures were prepared using MOLMOL (*72*) and MOLSCRIPT (*73*).

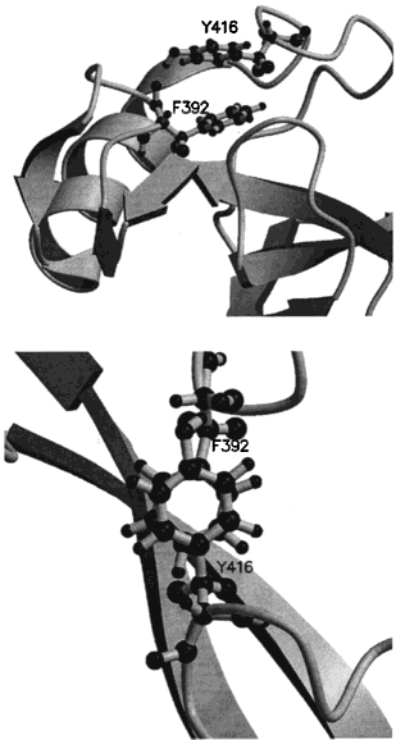

FIGURE 2: Two different views of the interaction of F392 (EF loop) and Y416 (BG loop) in the structure of uncomplexed p85 N-SH2. This arrangement is supported by NOESY signals between both phenyl rings and is observed in all structures of the structural ensemble.

and the central β-sheet (βB, βC, and βD). In agreement with the X-ray structure, the α-helices move closer to each other than suggested by the original NMR structure (also owing to the larger number of constraints in this NMR structure).

Both, the earlier and the present NMR structures show a similar conformation of the EF loop, different than that observed in the X-ray structure (*61*). In the X-ray structure the tip of the EF loop with F392 points more toward the +3 binding pocket even in the free SH2. In our NMR structure the loop seems more relaxed. There is an important consequence to the EF and BG loop conformations seen here. The side chains of residues F392 and Y416 are in close proximity to one another so that stacking appears to be likely (Figure 2). Stacking of the phenyl and the tyrosine rings is supported by several NOE contacts between the protons of the two rings.

Chemical Shift Perturbations in SH2−Peptide Complexes. We have previously shown that changes of chemical shifts in HSQC spectra caused by peptide binding can be correlated to binding sites and properties of the protein (*47*). In that work the effects of changing residues in the peptide ligand on chemical shift perturbations in the SH2 were used to map interactions with peptide ligands such as MT8/315pY (*47*).

Figure 3A depicts a comparison of ^{1}H and ^{15}N chemical shifts of the MT8/315pY− and MT15/315pY/322pY−SH2 complexes. The region of the primary pTyr binding site including αA and most parts of the central β-sheet showed chemical shifts very similar to those observed for the short MT peptides (blue). The only differences in the central β-sheet are observed for L372 and H385 (shown in red). Additional differences are observed in the EF loop (F392 and D394 shown in red), the αB helix, and the BG loop

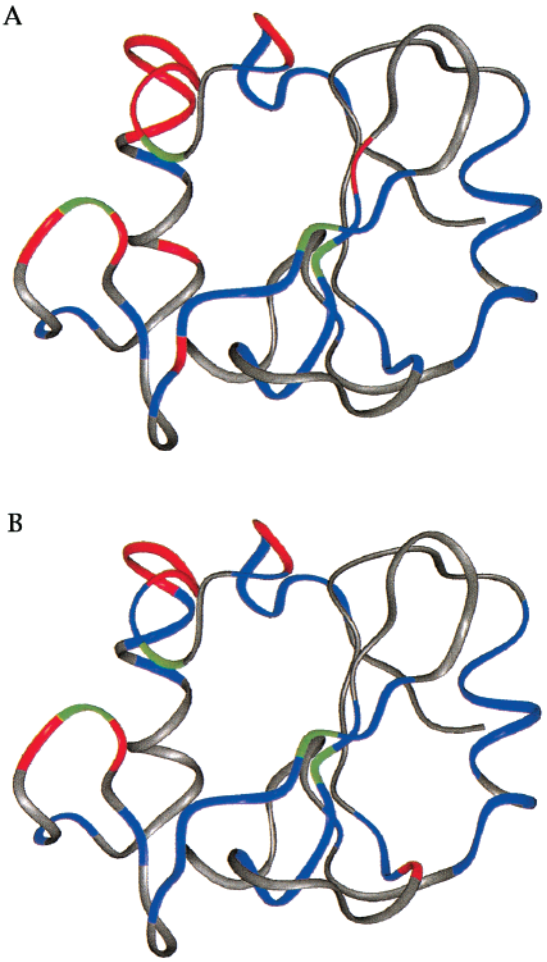

FIGURE 3: Ribbon diagrams of p85 N-SH2. Colors depict NH chemical shift changes. (A) Comparison of chemical shift perturbations upon binding of MT8/315pY vs MT15/315pY/322pY. Blue: Residues for which NMR signals are affected in the same way by both ligands. Red: Residues for which NMR signals are differently affected by each ligand. Green: Residues for which NMR signals disappear upon binding MT15/315pY/322pY. (B) Comparison of chemical shift perturbations upon binding of MT15/315pY vs MT15/315pY/322pY. Blue: Residues for which NMR signals are affected in the same way by both ligands. Red: Residues for which NMR signals are affected differently by each ligand. Green: Residues for which NMR signals disappear upon binding.

(V402,Y408−Q415, L420, and D421). To see the effect of the second phosphorylation, we compared the HSQCs of MT15/315pY and MT15/315pY/322pY. The differences observed in ^{1}H−^{15}N HSQC spectra are mostly small; they can be grouped in distinct regions, which are depicted in Figure 3B. Chemical shift differences between MT15/315pY and MT15/315pY/322pY were observed for the residues F392 and D394 in the EF loop and in BG loop residues N410−A414, L420, and D421 (red in Figure 3B). An additional difference is observed in residue A360, which is very sensitive to any changes in the protein or ligand. Several residues (green in Figure 3), including L370, I381, S393, and Y416, disappear upon addition of doubly phosphorylated peptide at 303 K. These signals even disappear upon addition of doubly phosphorylated peptide to a solution of p85 N-SH2 which is already bound to singly phosphorylated peptide. This observation suggests that MT15/315pY is displaced by MT15/315pY/322pY, which is consistent with the higher affinity of the doubly phosphorylated peptide observed in

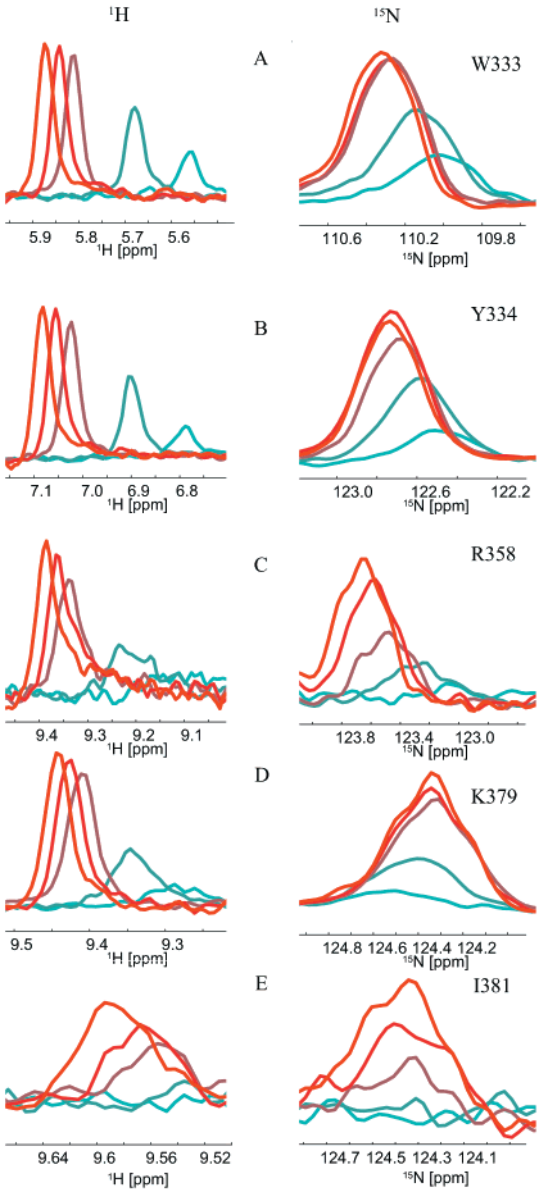

FIGURE 4: Effect of temperature variation on slices of ^{1}H−^{15}N HSQC spectra of the SH2−MT15/315pY/322pY complex recorded at 283, 293, 303, 308, and 311 K (cyan → red). W333 and Y334 show temperature-dependent line broadening. For R358, K379, and I381 multiple signal components are seen at low temperature which gradually disappear at higher temperature.

the peptide competition experiments. Interestingly, all four residues that disappear point toward the center of the +3 binding pocket (see below). Increasing the temperature to 311 K restored all four signals, and when the temperature was lowered to 283 K, a large number of additional signals disappeared.

Line Shapes in HSQC Spectra at Different Temperatures. To look more closely at the loss of signal observed for L370, I381, S393, and Y416, line shapes in one-dimensional slices of HSQC spectra were examined at different temperatures. Figure 4 shows ^{1}H and ^{15}N slices for I381 compared to a representative selection of residues which show different kinds of behavior. In simple cases, such as W333 and Y334, line shapes showed the typical behavior of lines narrowed by reduced viscosity of the protein solution at higher temperatures. Other signals such as R358 and K379 showed multiple signal components with small frequency separations at low temperature. In the proton dimension these signals melt into one single signal at higher temperature. However, in the ^{15}N dimension various signal components were observed even at higher temperature. For I381 a similar, but more dramatic effect was observed. Here the overall magnetization of the NH signal was distributed over a larger number of small signal components. Consequently, there was hardly any signal at 303 K. The signal became stronger at 308 K where two to three signal components are observed in both spectral dimensions. Signal component analysis applied to the FID also showed at least two to three signal components in the I381 signal at 311 K and at 308 K. Shoulders are better resolved in the ^{15}N dimension despite the presence of an unresolved NC$^\alpha$ coupling. This fine structure in the signal reflects the existence of different conformers. The coexistence of signals for one atom with a frequency separation of 20−30 Hz represents a typical case of slow exchange on a NMR time scale. The rate for the interconversion between signal components must be smaller than $\pi(\delta\nu/\sqrt{2})$, which is $<$50 Hz for a frequency separation of 20 Hz. The corresponding lifetime of the different states is $>$20 ms.

Slow exchange between different forms is also observed for some residues in the ligand in the ^{13}C{F_1}-filtered TOCSY and NOESY spectra (not shown). For example, pY11, the second phosphorylated tyrosine of the ligand is seen twice in the ^{13}C{F_1}-filtered TOCSY at 305 K. The HN frequency separation of the two spin systems is 0.285 ppm. The signals of M5, M7, I14, and L15 of the peptide are highly sensitive to temperature variations. For pY11 two sets of signals are even observed at 311 K. This shows that conformational heterogeneity involves the ligand as well as the protein.

C$^\alpha$ Chemical Shift Perturbation Caused by MT15/315pY/322pY Binding. Both chemical shift analysis and structural calculations have been used to examine the structure of the N-SH2−MT15/315pY/322pY complex. First C$^\alpha$ chemical shifts were examined. The correlation between chemical shifts and the secondary structure is much better established for C$^\alpha$ chemical shifts (*64*, *65*) than for NH chemical shifts because C$^\alpha$ chemical shifts correlate directly with the ϕ and χ_1 angles of the amino acid and are less dependent on other influences. C$^\alpha$ chemical shift changes upon ligand binding provide key information about rearrangements in the protein upon peptide binding. Although the analysis of C$^\alpha$ chemical shift perturbations is a common NMR approach, it has not usually been applied to study SH2 ligand binding.

Figure 5 shows differences in C$^\alpha$ resonances between free protein and the MT15/315pY/322pY complex. The general conclusion is that chemical shift differences in C$^\alpha$ resonances between free SH2 and SH2 binding MT15/315pY/322pY effectively map structural rearrangements where the ligand binds. The biggest chemical shift perturbations (red in Figure 6) occur for E411 (1.384 ppm), L413 (4.08 ppm), and A414 (2.28 ppm) in the BG loop. Other signals changing more than 0.5 ppm are A360 and D367 flanking the BC loop, G375 between βC and βD, K379 in βD, F392 in the EF loop region, V402, N410, S412, and L424 in αB, and the BG loop region. Smaller C$^\alpha$ chemical shift perturbations (0.4−0.5 ppm) were observed for S339, S380, and K382 (orange in Figure 6). Changes of 0.3−0.4 ppm (yellow in Figure 6) were found for additional residues in the central β-sheet

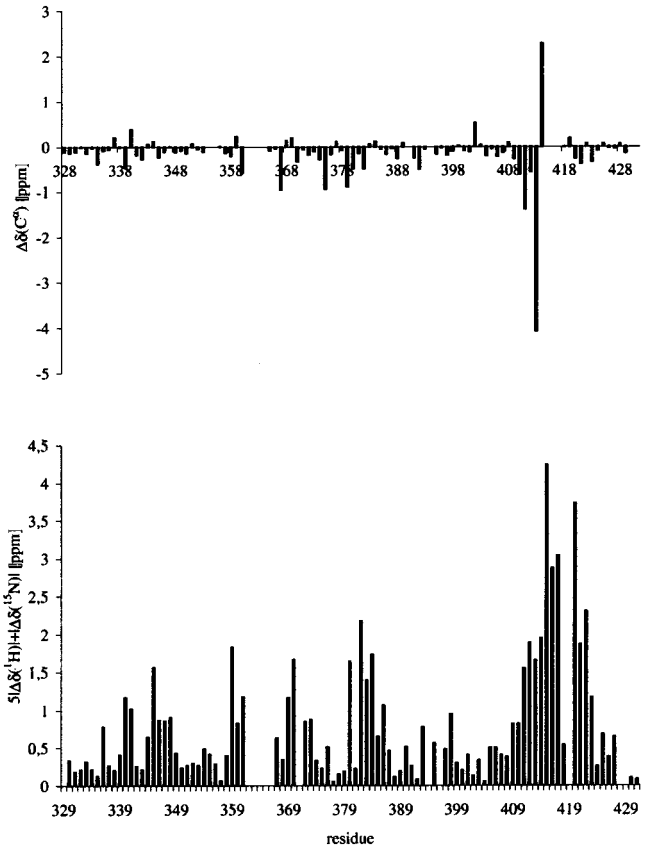

FIGURE 5: Chemical shift differences induced by adding MT15/315pY/322pY to uncomplexed p85 N-SH2. Top: Differences of C^{α} chemical shifts. Bottom: Combined value for chemical shift perturbations in $^{1}H-^{15}N$ HSQC spectra ($5 \times |\Delta\delta(^{1}H)| + |\Delta\delta(^{15}N)|$).

(Y334 in βA, L370 in βC), at the lower αA helix (R340), in αB (N406), and in the BG loop (D421 and K423).

SH2−MT15/315pY/322pY Complex: Structure Calculation. Figure 6 shows the 20 best structure backbones obtained after distance geometry and energy minimization for the complex between the p85 N-SH2 and the MT15/315pY/322pY. The RMSD calculated with the BC loop is 1.96 ± 0.26 Å for all atoms and 1.22 ± 0.19 Å for the backbone; without the BC loop a value of 1.81 ± 0.25 Å is obtained for all atoms and 1.12 ± 0.19 Å for the protein backbone. To improve the quality of the structure, NOESY spectra recorded at two different temperatures, 305 and 311 K, were used for the structure calculation. This was necessary to overcome the lack of distance constraints for key residues such as I381 (βD5) with increased line widths at lower temperatures. A total of 2050 NOESY constraints were identified within the protein. Fifty-three distance constraints between the $^{13}C-^{15}N$-labeled protein and the unlabeled peptide were identified in $^{13}C\{F_1\}$-filtered 2D NOESY spectra, mostly between side chains.

Fifty-three constraints observed between the ligand and the SH2 is a substantial number, since a lack of intramolecular distance constraints is a common problem in NMR structural analysis. They were sufficient to define the location of the peptide, but the detailed location of the peptide side chains was not very well defined. For example, even though there were constraints to the phenyl ring, the pTyr phosphate group does not provide any constraints. The limited number of constraints inevitably caused some uncertainty in the structure, which is reflected in the increased RMSD compared to the free protein.

To overcome the lack of constraints for the primary (315) phosphotyrosine, phosphate interactions, known from X-ray structures (e.g., ref *61*) involving the phosphate and the phenyl ring of the primary phosphotyrosine were used as constraints for the structure calculation (as shown in Table 2A). These constraints included such conserved hydrogen bonds as formed by the oxygens of the phosphate with R340 and R358. Our own constraints derived from the $^{13}C\{F_1\}$-filtered NOESY in the primary phosphotyrosine binding pocket (Table 2B) are in good agreement with the position of the phosphotyrosine in other SH2 structures. Ambiguities in the assignment of the 2D $^{13}C\{F_1\}$-filtered NOESY spectrum, which correlates $H^{12}C$ of the ligand with $H^{13}C$ of the protein, could not be resolved by editing the ^{13}C-filtered NOESY in a third dimension because of limited signal to noise. For this reason, chemical shift perturbations in ^{15}N

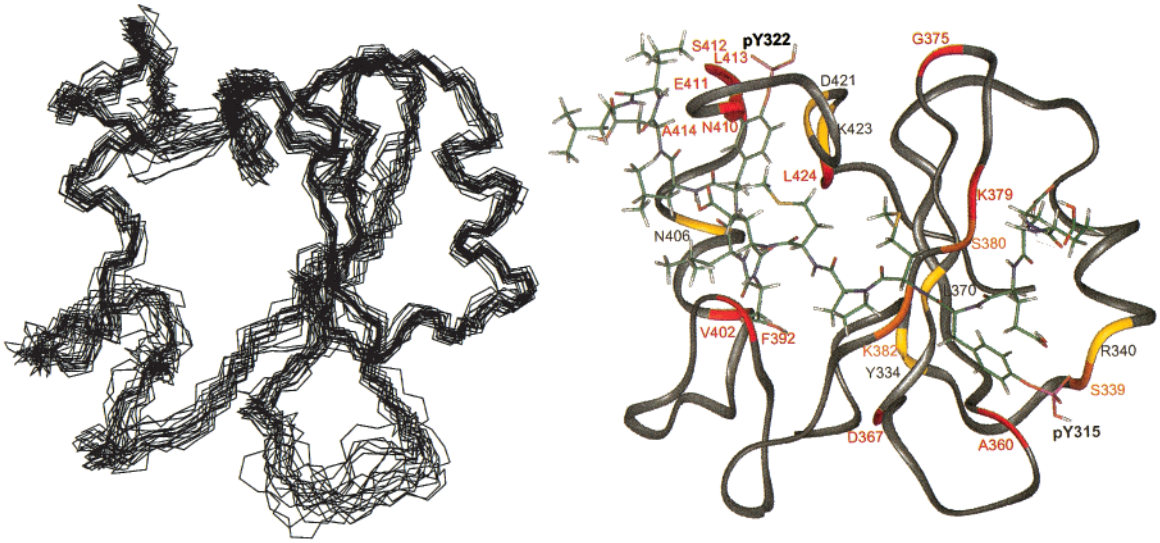

FIGURE 6: Left: Superposition of 20 structures of the p85 N-SH2−MT15/315pY/322pY complex after DYANA and energy minimization (ligand not shown). Right: Structure of the p85 N-SH2−MT15/315pY/322pY complex. Colors indicate C^{α} chemical shift perturbations: red > 0.5 ppm, orange > 0.4 ppm, and yellow > 0.3 ppm.

Table 2: (A) Distance Constraints Derived from X-ray Structures Used for Structure Calculation and (B) NOESY-Derived Distance Constraints Involving the pTyr Binding Site

(A) Distance Constraints Derived from X-ray Structures	
phosphopeptide	SH2
Y315-phosphate	R340 HH
Y315-phosphate	R358 HH
Y315-phosphate	A360 HB
Y315-phosphate	S361 OH
Y315-phosphate	T362 HG
(B) NOESY-Derived Distance Constraints	
MT15/315pY/322pY	SH2
Y315 phenyl	R358 HG
Y315 phenyl	R358 HD
Y315 phenyl	R358 HE
Y315 phenyl	D359 HN
Y315 phenyl	T369 HG
Y315 phenyl	S380 HB
Y315 HA	I381 HG
Y315 HB	K382 HD
Y315 phenyl	K382 HD

HSQCs were used to assign potential binding partners in the protein.

A clear picture of the interaction of the doubly tyrosine phosphorylated peptide with the SH2 emerges from chemical shift analysis and structure determination. The peptide stretches from the primary phosphotyrosine binding site over the central β-sheet to the BG loop where the second pTyr interacts with several loop residues. Conformational changes in the primary pTyr binding site are seen in C^{α} chemical shift changes of S339 and R340 in the lower αA helix and of A360 and D367 flanking the BC loop. This region rearranges to form the pTyr binding pocket. However, on the basis of comparison of chemical shift perturbations between MT8/315pY and MT15/315pY/322pY, the structure around the primary 315 phosphorylation site of the ligand is quite similar to the complex with a shorter singly phosphorylated peptide. The chemical shift perturbation of A360 with MT15/315pY/322pY in this region is superficially unexpected because the primary pTyr binding site is not affected by phosphorylation of the second tyrosine. However, because of conformational flexibility of the BC loop the resonance of A360 is very sensitive to any change in the protein or peptide.

The peptide bends at pTyr to cross the central β-sheet. Conformational changes in the central β-sheet are caused by steric requirements of the peptide. Specific interactions between the backbone and the side chains of +1 and +3 in the peptide involve rearrangements in K379, S380, and K382. Secondary effects are seen in other strands of the sheet such as C^{α} chemical shift changes in Y334 in βA and L370 in βD. G375 between βC and βD changes its conformation because the whole β-sheet moves together, becoming more compact. As a result, the long ligand has enough room to bend between the β-sheet and αB, before it can emerge toward the BG loop. The M + 1 side chain is coordinated through hydrophobic contacts with the side chains of K379, I381, K419, and L420.

The protein adapts to the binding of the peptide by rearranging the EF and BG loops toward the bulk of the protein. The BG loop presumably rearranges because of bulky groups (leucines and isoleucine in the C-terminus of the peptide). As a consequence, the αB helix is distorted at its C-terminal end. This is in good agreement with the observed C^{α} chemical shift changes which were particularly strong in the end of αB and the lack of HN−HN NOESY signals which are typical for α-helices.

The C^{α} chemical shift change of V402 indicates the position where the peptide bends toward the BG loop because of steric requirements. V402 is nevertheless displaced. Residues N410−A414 and D421 and K423 in the BG loop show significant differences. The C-terminus of αB moves toward what is seen as the back of the protein in Figure 6, so that the α-helices of complexed and free SH2 are at an angle of 5° with respect to one another.

The EF loop in the complex structure resembles the conformation reported in the X-ray structure (*61*). The tip of the loop is oriented toward the +3 pocket. The most dramatic conformational change upon peptide binding seen in the X-ray structure is rotation of the side chain of Y416 (BG5) about χ_1. In these NMR structures the phenolic hydroxyl group of Y416 has moved 8 Å between free and complex conformations. The C^{α} position also moves 5 Å. The result of this movement, which unstacks F392 from Y416, is to open the +3 hydrophobic pocket and to move F392 at the tip of the EF loop toward the peptide. This is in good agreement with the large chemical shift change observed for the amide of Y416 [$\Delta\delta(^{15}N) = 3.01$ ppm]. A conformational change in the backbone of the BG loop is clearly observed.

Rearrangements in the BG loop are important for +3 coordination. The structure shows hydrophobic contacts with I381, L413, A414, K419, and L420. All of these residues also showed strong chemical shift perturbations upon binding MT15/315pY/322pY (Figure 5). Not only are K419 and L420 contacting both +1 and +3, but they are also affected by the C-terminus of the peptide, since chemical shift changes of K419 and L420 differ in complexes with MT8/315pY and MT15/315pY.

The C-terminus of the doubly phosphorylated MT peptide is bound in a mode that has not been seen with previous SH2 domain structures. The second phosphotyrosine (322) is coordinated by the BG loop and the C-terminal part of αB. The minimized structure suggests a network of hydrogen bonds which links the oxygens of the phosphate with the backbone amides of E411 and S412 and with the side chain amides of K423 as shown in Figure 7. The side chain of K423 is the only positively charged binding partner possible for the pTyr oxygens. Hydrophobic contacts are made with L404, Y408, L413, L420, and L424. The importance of all of these residues for MT15/315pY/322pY is supported by small chemical shift changes resulting from addition of doubly phosphorylated MT peptide in comparison to chemical shifts of singly phosphorylated peptide. The structure suggests hydrogen bonds from D394 to the amide of +6 leucine and from F392 to the side chain carboxyl of +4 glutamate that appear to be significant for orienting the residues between +3 and the second pTyr. At D9 (+5) the peptide changes its direction, bending about 80°, so that it is parallel to the αB helix.

DISCUSSION

Most attention to the interaction of peptides containing two phosphotyrosines with SH2 domains has focused on the

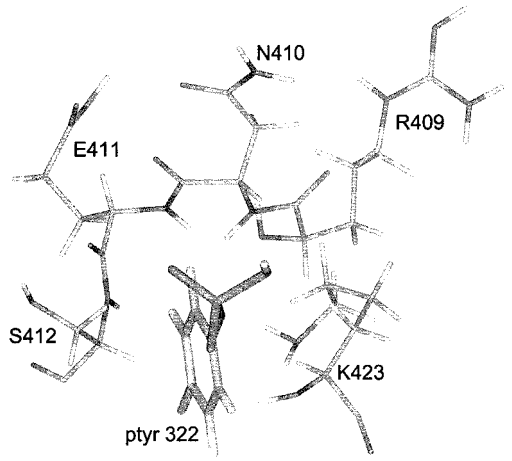

FIGURE 7: Coordination of the pTyr 322 in representative structures of the p85 N-SH2−MT15/315pY/322pY complex.

idea that the two tyrosine phosphorylated sequences interact with different SH2 domains in the target protein. Experiments here comparing the behavior of isolated single N-SH2 and C-SH2 domains of the p85 regulatory PI3K subunit showed that they behaved differently with respect to binding polyoma virus MT sequences. It is clear that phosphotyrosine 315 of MT is the major binding site for PI3K (*22*). Either N-SH2 or C-SH2 can bind this sequence. However, tyrosine 322 of polyoma middle T can also be phosphorylated. Competition experiments showed that this second phosphorylation has no significant effect on the ability of a MT peptide to interact with the C-SH2. However, the doubly phosphorylated peptide showed nearly 10-fold higher binding to the isolated N-SH2 domain.

NMR structural analysis was undertaken to try to understand the difference in affinity arising from the second phosphate. The interaction of the N-SH2 with the doubly phosphorylated MT sequences was also examined by analyzing chemical shift perturbations. The two methods have provided complementary insights into the nature of the interactions. There was no indication in our NMR spectra of dimerization of the SH2 domain caused by the second phosphotyrosine. Therefore, the doubly phosphorylated ligand bound with increased affinity to a single SH2. The NMR results provided a satisfying explanation for the binding of the second phosphotyrosine to the N-SH2 structure. Our results therefore indicate a novel mode of interaction for SH2 domains and doubly tyrosine phosphorylated sequences.

To understand the structure of the SH2−phosphopeptide complex, the structure of the free SH2 was first determined. The rat N-SH2 variant used in these studies had serine instead of leucine at the position corresponding to residue 380 in human p85. The structure of the free SH2 showed some differences from known NMR and X-ray structures in some positions. As noted earlier, differences between this NMR structure and that of Hensmann (*60*) are likely to be a consequence of improving NMR technology. The NMR structure here presents a clearer picture of the BG loop and is in accordance with Nolte's X-ray structure. It explains why the side chains in the +1 position in the ligand (e.g., Val in peptides derived from PDGFr) cause particularly large changes in chemical shift perturbations for residues K419 and L420 in the BG loop. This structure shows that the fold

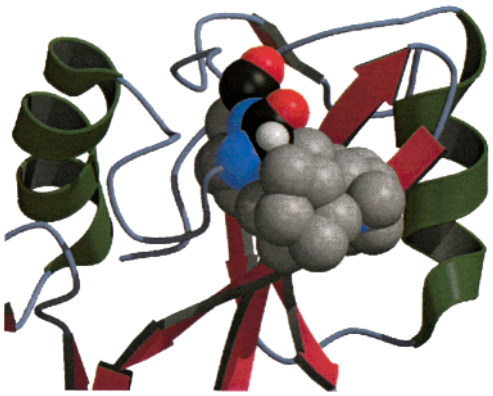

FIGURE 8: Interaction of K379, K419, and L420 in the uncomplexed p85 N-SH2.

of the BG loop brings these two residues in direct contact with K379 in the upper part of the central β-sheet to form a hydrophobic surface for +1 side chain interactions (Figure 8).

Both the present and earlier NMR structures show differences in the EF loop region from the X-ray structure. The differences have an important consequence seen in our structure. The EF loop folds so that the phenyl rings of F392 and Y416 are stacked (Figure 2). In the peptide complex Y416 is no longer stacked with F392. The observation of stacking would explain previous chemical shift perturbation data. F392 and its surrounding residues titrate upon binding of peptide. Titration of a Y416A mutant of the p85 N-SH2 showed little or no chemical shift perturbations for F392 (U. Günther, unpublished results). Surprisingly, the Y416A mutant showed a binding affinity similar to that of wild type. It will be of interest to determine whether this stacking interaction affects specificity for particular ligands.

The SH2−ligand complex presented here has a longer C-terminal extension compared to previous structural studies of SH2−ligand interactions. The second phosphotyrosine is at position +7 with respect to the first. A major challenge in such studies is identifying contacts between the ligand and the protein. For example, even after developing new methods to identify such contacts (*66*), Tsuchiya and colleagues (*67*) were not able to establish contacts between an epidermal growth factor receptor peptide and the Grb2 SH2. Our efforts met with more success. For ambiguous peaks, chemical shift perturbations were used to distinguish possible assignments. It was thus possible to assign ^{13}C-filtered TOCSY and NOESY spectra.

Chemical shift perturbations clearly implicated the BG loop in additional interactions with MT15/315pY/322pY. The location of the C-terminus of the peptide in the complex is supported by a series of NOESY contacts, despite the lack of direct data for the phosphate oxygens. Efforts to use the phosphate signal for additional NMR experiments failed owing to the broadness of its resonance and the fact that their resonance frequencies are degenerate.

The C-terminus of the peptide is relocated from EF toward BG compared to the SH2 complex structures determined by Nolte (*61*). This allows pTyr 322 (position 11 of the peptide) to interact with the positively charged K423. The C-SH2 has a Thr in this position and no other positively charged side chain nearby which would potentially adopt the role of K423. This probably explains why increased affinity for

doubly phosphorylated peptide is observed only for the N-SH2 domain. A series of hydrophobic side chains in the BG loop provide a surface for interaction with the bulky hydrophobic residues after pY11. At present, it is not clear whether the second phosphate also affects these interactions.

Perhaps the most astonishing observation in this work is the behavior of line shapes of NMR signals in different positions of the SH2. Line shapes became very complex when there is a second tyrosine phosphorylation in the bound peptide. The possibility that this was caused by sample heterogeneity of the ligand was eliminated by ESI and MALDI mass spectroscopy. Even if the sample was stored at room temperature in aqueous solution, the ligand was stable.

Thus the observed line shapes are an unambiguous indication of the presence of multiple conformers in slow exchange. There must be an equilibrium of different conformers with similar energies which exchange slowly because of an energy barrier between the different forms. The close proximity of the signal components suggests a similar magnetic environment. Most residues involved in such conformational exchange processes are directly involved in the interaction with the peptide through their side chains. For this reason, it is not surprising that conformational lability was also observed in the ligand.

The presence of different types of line shapes in the same protein shows that conformational heterogeneity is limited to certain regions. Since the singly phosphorylated peptide does not introduce conformational heterogeneity, it must be the second pTyr interaction that is responsible.

Additional complexity arises from the fact that raising the temperature reveals multiple forms in slow exchange for residues such as I381 and to some degree R358 and K379. Clearly, we do not observe a transition from intermediate to fast exchange when raising the temperature. One possible explanation is that signals from a large number of conformers become too weak to be observed at low temperature. As the temperature is raised, signals sharpen because the correlation time of the protein is reduced. Exchange rates will also increase, and consequently, conformers with relatively small energy barriers will melt into one signal. Thus the overall number of conformers is reduced. The presence of multiple signal components even at 311 K indicates that slow conformational averaging on a millisecond time scale is present.

There is more than one possible interpretation of the observation of conformational heterogeneity. In one view, the unliganded protein has conformational exchange on a rapid time scale. The exchange between conformers could be slowed by interaction of the second pTyr so they become detectable. It is even possible that the doubly phosphorylated ligand interacts favorably with SH2 conformers that never give productive binding with a peptide that is singly phosphorylated. However, since heterogeneity was not observed in the free SH2 or in the single pTyr complex, and given the demonstration of the second pTyr binding site, we favor the explanation that the formation of conformers is triggered by the second pTyr.

An ensemble of energetically equal or similar conformers which all bind the ligand with comparable affinity may cause an increase in entropy, and thus the overall affinity is higher. However, it seems unlikely that this gain of affinity would compensate losses from conformational flexibility. This may be the reason phosphorylation of tyrosine 322 causes an increase of affinity of only 1 order of magnitude. Previous data showed that removing phosphate from tyrosine 315 reduced binding 3 orders of magnitude (*47*). This difference may be biologically relevant. The 322 sequence can be involved in other interactions (PLCγl) resulting in an equilibrium between different interactions. This sort of interpretation is supported by a recent isothermal titration calorimetry study by O'Brien et al., which suggests that an individual doubly phosphorylated binding site which interacts with SH2 domains can recruit different proteins (*68*).

In conclusion, this work demonstrates that SH2 domains can have a second, nontraditional phosphotyrosine binding site. This may well be relevant to earlier observations that SH2 domains can interact with non-phosphotyrosine-containing peptides in a phosphorylation-dependent manner (*69*, *70*). For this SH2, the challenge from the structural studies is to go back to new genetic and biological analysis to assess the real importance of this novel mode of interaction and to probe the role of conformational behavior by additional NMR experiments.

ACKNOWLEDGMENT

We thank H. Rüterjans for kindly giving U. Günther access to his laboratory.

REFERENCES

1. Vanhaesebroeck, B., and Waterfield, M. (1999) *Exp. Cell Res. 253*, 239−254.
2. Dankort, D., and Muller, W. (2000) *Oncogene 19*, 1038−1044.
3. Datta, S., Brunet, A., and Greenberg, M. (1999) *Genes Dev. 13*, 2905−2927.
4. Wurmser, A., Gary, J., and Emr, S. (1999) *J. Biol. Chem. 274*, 9129−9132.
5. Rameh, L., and Cantley, L. (1999) *J. Biol. Chem. 274*, 8347−8350.
6. Corvera, S., D'Arrigo, A., and Stenmark, H. (1999) *Curr. Opin. Cell Biol. 11*, 460−465.
7. Wymann, M., and Pirola, L. (1998) *Biochim. Biophys. Acta 1436*, 127−150.
8. Krugmann, S., and Welch, H. (1998) *Curr. Biol. 8*, R828.
9. Fruman, D., Meyers, R., and Cantley, L. (1998) *Annu. Rev. Biochem. 67*, 481−507.
10. Fantl, W. J., Escobedo, J. A., Martin, G. A., Turck, C. W., del Rosario, M., McCormick, F., and Williams, L. T. (1992) *Cell 69*, 413−423.
11. Valius, M., Bazenet, C., and Kazlauskas, A. (1993) *Mol. Cell. Biol. 13*, 133−143.
12. Derman, M. P., Toker, A., Hartwig, J. H., Spokes, K., Falck, J. R., Chen, C. S., Cantley, L. C., and Cantley, L. G. (1997) *J. Biol. Chem. 272*, 6465−6470.
13. Wennstrom, S., Hawkins, P., Cooke, F., Hara, K., Yonezawa, K., Kasuga, M., Jackson, T., Claesson-Welsh, L., and Stephens, L. (1994) *Curr. Biol. 4*, 385−393.
14. Meili, R., Ellsworth, C., Lee, S., Reddy, T., Ma, H., and Firtel, R. (1999) *EMBO J. 18*, 2092−2105.
15. Kucera, G., and Rittenhouse, S. (1990) *J. Biol. Chem. 265*, 5345−5348.
16. Nolan, R. D., and Lapetina, E. G. (1990) *J. Biol. Chem. 265*, 2441−2445.
17. Traynor-Kaplan, A. E., Thompson, B. L., Harris, A. L., Taylor, P., Omann, G. M., and Sklar, L. A. (1989) *J. Biol. Chem. 264*, 15668−15673.
18. Ninomiya, N., Hazeki, K., Fukui, Y., Okada, T., Hazeki, O., and Ui, M. (1994) *J. Biol. Chem. 269*, 22732−22737.
19. Minshall, C., Arkins, S., Freund, G., and Kelley, K. (1996) *J. Immunol. 156*, 939−947.

20. Shaw, L., Rabinovitz, I., Wang, H., Toker, A., and Mercurio, A. (1997) *Cell 92*, 949−960.
21. Carpenter, C., Duckworth, B., Auger, K., Cohen, B., Schaffhausen, B., and Cantley, L. (1990) *J. Biol. Chem. 265*, 19704−19711.
22. Yoakim, M., Hou, W., Liu, Y., Carpenter, C. L., Kapeller, R., and Schaffhausen, B. S. (1992) *J. Virol. 66*, 5485−5491.
23. Escobedo, J. A., Kaplan, D. R., Kavanaugh, W. M., Turck, C. W., and Williams, L. T. (1991) *Mol. Cell. Biol. 111*, 125−132.
24. Kashishian, A., Kazlauskas, A., and Cooper, J. (1992) *EMBO J. 11*, 1373−1382.
25. Cohen, G., Ren, R., and Baltimore, D. (1995) *Cell 88*, 237−248.
26. Sawyer, T. (1998) *Biopolymers 47*, 243−261.
27. Marengere, L. E., and Pawson, T. (1994) *J. Cell Sci., Suppl. 18*, 97−104.
28. Schaffhausen, B. (1995) *Biochim. Biophys. Acta 1242*, 61−75.
29. Cantley, L. C., and Songyang, Z. (1994) *J. Cell Sci., Suppl. 18*, 121−126.
30. Kuriyan, J., and Cowburn, D. (1997) *Annu. Rev. Biophys. Biomol. Struct. 26*, 259−288.
31. Flaswinkel, H., Barner, M., and Reth, M. (1995) *Semin. Immunol. 7*, 21−27.
32. Cambier, J. (1995) *J. Immunol. 155*, 3281−3285.
33. Harvey, R., Oostra, G. L., Belsham, G. J., Gillett, P., and Smith, A. E. (1984) *Mol. Cell. Biol. 4*, 1334−1342.
34. Schaffhausen, B., and Benjamin, T. (1981) *J. Virol. 40*, 184−196.
35. Hunter, T., Hutchinson, M., and Eckhart, W. (1984) *EMBO J. 3*, 73−80.
36. Kaplan, D., Whitman, M., Schaffhausen, B., Raptis, L., Garcea, R., Pallas, D., Roberts, T., and Cantley, L. (1986) *Proc. Natl. Acad. Sci. U.S.A. 83*, 3624−3628.
37. Whitman, M., Kaplan, D., Schaffhausen, B., Cantley, L., and Roberts, T. (1985) *Nature 315*, 239−242.
38. Su, W., Liu, W., Schaffhausen, B. S., and Roberts, T. M. (1995) *J. Biol. Chem. 270*, 12331−12334.
39. Futterer, K., Wong, J., Grucza, R. A., Chan, A. C., and Waksman, G. (1998) *J. Mol. Biol. 281*, 523−537.
40. Hatada, M. H., Lu, X., Laird, E. R., Green, J., Morgenstern, J. P., Lou, M., Marr, C. S., Phillips, T. B., Ram, M. K., Theriault, K., *et al. (1995) Nature 376*, 32−*38.*
41. Mayer, B. (1995) *Structure 3*, 977−980.
42. Herbst, R., Andrews, G., Contillo, L., Lamphere, L., Gardner, J., Lienhard, G., and Gibbs, E. (1994) *Biochemistry 33*, 9376−9381.
43. Carpenter, C. L., Auger, K. R., Chanudhuri, M., Yoakim, M., Schaffhausen, B., Shoelson, S., and Cantley, L. C. (1993) *J. Biol. Chem. 268*, 9478−9483.
44. Backer, J., Myers, M., Jr., Shoelson, S., Chin, D., Sun, X., Miralpeix, M., Hu, P., Margolis, B., Skolnik, E., and Schlessinger, J. (1992) *EMBO J. 11*, 3469−3479.
45. Rordorf-Nikolic, T., Van Horn, D. J., Chen, D., White, M. F., and Backer, J. M. (1995) *J. Biol. Chem. 270*, 3662−3666.
46. Layton, M. J., Harpur, A. G., Panayotou, G., Bastiaens, P. I., and Waterfield, M. D. (1998) *J. Biol. Chem. 273*, 33379−33385.
47. Günther, U., Liu, Y., Sanford, D., Bachovchin, W., and Schaffhausen, B. (1996) *Biochemistry 35*, 15570−15581.
48. Yoakim, M., Hou, W., Songyang, Z., Liu, Y., Cantley, L., and Schaffhausen, B. (1994) *Mol. Cell. Biol. 14*, 5929−5938.
49. Driscoll, P. C., Clore, G. M., Marion, D., Wingfield, P. T., and Gronenborn, A. M. (1990) *Biochemistry 29*, 3542−3556.
50. Marion, D., Driscoll, P. C., Kay, L. E., Wingfield, P. T., Bax, A., Gronenborn, A. M., and Clore, G. M. (1989) *Biochemistry 28*, 6150−6156.
51. Ikura, M., Kay, L. E., and Bax, A. (1990) *Biochemistry 29*, 4659−4667.
52. Bax, A., and Ikura, M. (1991) *J. Biomol. NMR 1*, 99−104.
53. Kuboniwa, H., Gresziek, S., Delaglio, F., and Bax, A. (1994) *J. Biomol. NMR 4*, 871−878.
54. Bax, A., Clore, G. M., and Gronenborn, A. M. (1990) *J. Magn. Reson. 88*, 425−431.
55. Pristovsek, P., and Kidric, J. (1997) *Biopolymers 42*, 671−679.
56. Gemecker, G., Olejniczak, E., and Fesik, S. (1992) *J. Magn. Reson. 96*, 199−204.
57. Petros, A., Kawai, M., Luly, J., and Fesik, S. (1992) *FEBS Lett. 308*, 309−314.
58. . Freund, R., Dawe, C. J., Carrol, J. P., and Benjamin, T. L. (1992) *Am. J. Pathol. 141*, 1409−1425.
59. Carmichael, G., Schaffhausen, B., Mandel, G., Liang, T., and Benjamin, T. (1984) *Proc. Natl. Acad. Sci. U.S.A. 81*, 679−683.
60. Hensmann, M., Booker, G. W., Panayotou, G., Boyd, J., Linacre, J., Waterfield, M., and Campbell, I. D. (1994) *Protein Sci. 3*, 1020−1030.
61. Nolte, R. T., Eck, M. J., Schlessinger, J., Shoelson, S. E., and Harrison, S. C. (1996) *Nat. Struct. Biol. 3*, 364−374.
62. Songyang, Z., Shoelson, S., Chaudhuri, M., Gish, G., Pawson, T., Haser, W., King, F., Roberts, T., and Ratnofsky, S. (1993) *Cell 72*, 767−778.
63. Booker, G. W., Breeze, A. L., Downing, A. K., Panayotou, G., Gout, I., Waterfield, M. D., and Campbell, I. D. (1992) *Nature 358*, 684−687.
64. Oldfield, E. (1995) *J. Biomol. NMR 5*, 217−225.
65. Wishart, D. S., Bigam, C. G., Yao, J., Abildgaard, F., Dyson, H. J., Oldfield, E., Markley, J. L., and Sykes, B. D. (1995) *J. Biomol. NMR 6*, 135−140.
66. Ogura, K., Terasawa, H., and Inagaki, F. (1996) *J. Biomol. NMR 8*, 492−498.
67. Tsuchiya, S., Ogura, K., Hatanaka, H., Nagata, K., Terasawa, H., Mandiyan, V., Schlessinger, J., Aimoto, S., Ohta, H., and Inagaki, F. (1999) *J. Biochem. 125*, 1151−1159.
68. O'Brien, R., Rugman, P., Renzoni, D., Layton, M., Handa, R., Hilyard, K., Waterfield, M., Driscoll, P., and Ladbury, J. (2000) *Protein Sci. 9*, 570−579.
69. Cleghorn, V., and Mossison, D. (1994) *J. Biol. Chem. 269*, 17749−17755.
70. Pendergast, A. M., Muller, A. J., Havlik, M. H., Maru, Y., and White, O. N. (1991) *Cell 66*, 161−171.
71. Eck, M. J., Shoelson, S. E., and Harrison, S. C. (1993) *Nature 362*, 87−91.
72. Koradi, R., Billeter, M., and Wüthrich, K. (1996) *J. Mol. Graphics 14*, 51−55.
73. Kraulis, P. (1991) *J. Appl. Crystallogr. 24*, 946−950.

BI001474D